HHS Public Access

Author manuscript

Chem Res Toxicol. Author manuscript; available in PMC 2015 April 10.

Published in final edited form as:

Chem Res Toxicol. 2005 September ; 18(9): 1339–1346. doi:10.1021/tx050147+.

Recognition and Incision of γ-Radiation-Induced Cross-Linked Guanine—Thymine Tandem Lesion G[8,5-Me]T by UvrABC Nuclease

Zhengguan Yang[†], **Laureen C. Colis**[‡], **Ashis K. Basu**[*,‡], and **Yue Zou**[*,†]

[†]Department of Biochemistry and Molecular Biology, James H. Quillen College of Medicine, East Tennessee State University, Johnson City, Tennessee 37604

[‡]Department of Chemistry, University of Connecticut, Storrs, Connecticut 06269

Abstract

Nucleotide excision repair (NER) plays an important role in maintaining the integrity of DNA by removing various types of bulky or distorting DNA adducts in both prokaryotic and eukaryotic cells. In *Escherichia coli*, the excision repair proteins UvrA, UvrB, and UvrC recognize and incise the bulky DNA damages induced by UV light and chemical carcinogens. In this process, when a putative lesion in DNA is identified initially by UvrA, a subsequent strand opening is carried out by UvrB that not only ensures that the distortion is indeed due to a damaged nucleotide but also recognizes the chemical structure of the modified nucleotides with varying efficiencies. UvrB also recruits UvrC that catalyzes both the 3′ and the 5′-incisions. Herein, we examined the interaction of UvrABC with a DNA substrate containing a single G[8,5-Me]T cross-link and compared it with T[6,4]T (the 6-4 pyrimidine–pyrimidone photoproduct) and the C8 guanine adduct of *N*-acetyl-2-aminofluorene (AAF). The intrastrand vicinal cross-link G[8,5-Me]T containing a covalent bond between the C8 position of guanine and the 5-methyl carbon of the 3′-thymine is formed by X-radiation, while T[6,4]T is a vicinal cross-link induced by the UV light. We also selected the AAF adduct for comparison because it represents a highly distorting monoadduct containing a covalent linkage at the C8 position of guanine. The dissociation constants (K_d) for UvrA protein binding to DNA substrates containing the G[8,5-Me]T, T[6,4]T, and AAF adducts, as determined by gel mobility shift assays, were 3.1 ± 1.3, 2.8 ± 0.9, and 8.2 ± 1.9, respectively. Although UvrA had a considerably higher affinity for G[8,5-Me]T than for the AAF adduct, the G[8,5-Me]T intrastrand cross-link was incised by UvrABC much less efficiently than the T[6,4]T intrastrand cross-link and the AAF adduct. Similar incision results also were obtained with the DNA substrates containing the adducts in a six-nucleotide bubble, indicating that the inefficient incision of G[8,5-Me]T cross-link by UvrABC was probably due to the lack of efficient recognition of the adduct by UvrB at the second step of DNA damage recognition in the *E. coli* NER. Indeed, as compared to T[6,4]T and AAF substrates, which clearly showed UvrB–DNA complex formation, very little

[*]To whom correspondence should be addressed. (Y.Z.) Tel: 423-439-2124. Fax: 423-439-2030. E-mail: zouy@etsu.edu. (A.K.B.) Tel: 860-486-3965. Fax: 860-486-2981. ashis.basu@uconn.edu.

Supporting Information Available: Preparation of G[8,5]T-51bp, T[6,4]T-49bp, AAF-50bp, and nondamaged DNA substrates; and ESI-MS spectra of G[8,5-Me]T deoxydinucleoside monophosphate and cross-linked 12-mer. This material is available free of charge via the Internet at http://pubs.acs.org.

UvrB complex was detectable with the G[8,5-Me]T substrate. Our result suggests that G[8,5-Me]T intrastrand cross-link is more resistant to excision repair in comparison with the T[6,4]T and AAF adducts and thus will likely persist longer in *E. coli* cells.

Introduction

Ionizing radiation generates a wide array of lesions in DNA, including single and double strand breaks, base damages, and apurinic/apyrimidinic sites (1). A vast majority of these DNA damages are indistinguishable from those formed under endogenous oxidative stress (2). The formation of clustered DNA damages within a short stretch of DNA, however, is a unique feature of ionizing radiation (3). A group of free radical-induced tandem lesions, including the cross-link in which the guanine C8 is covalently linked to the methyl carbon of an adjacent thymine (G[8,5-Me]T),[1] are formed following X-irradiation of oxygen-free aqueous solution of DNA (4–8). The G[8,5-Me]T tandem lesion represents one in a series of nearly a dozen radiation-induced purine–pyrimidine (or pyrimidine–purine) cross-links identified in the past decade (9).

The biological effects of these intrastrand vicinal cross-links are little studied, except for a report that a cross-link formed by guanine and cytosine causes misreplication in vitro (5). To our knowledge, repairability of these cross-links, either in vitro or in vivo, has not yet been explored. Most ionizing radiation/oxidation-induced damages are repaired by DNA glycosylases (i.e., base excision repair) (ref 10 and references therein). However, 8,5′-cyclopurine-2′-deoxynucleosides, which belong to a group of radiation-induced tandem damages that strongly block gene expression, are repaired by nucleotide excision repair (NER) (11). The vicinal cross-links such as G[8,5-Me]T are structurally distinct from various other damages induced by X-radiation. Intrastrand cross-links are known to induce bends in DNA, which may serve as an initial recognition feature for repair systems such as the NER. It is therefore conceivable that G[8,5-Me]T and related radiation-induced cross-links that are likely to induce kinks or bends in DNA may also be repaired by NER.

The general mechanism of UvrABC nuclease, the NER proteins of *Escherichia coli*, is now well-established (1), even though details of this process continue to be investigated by many research groups. It is known that the UvrA and UvrB proteins are involved in recognition of a lesion in DNA, whereas UvrC performs the incisions. When a putative lesion is identified initially by UvrA, a subsequent strand opening is carried out by UvrB that ensures that the distortion is indeed due to a damaged nucleotide (12, 13). It is believed that the β-hairpin domain of UvrB is inserted into the DNA helix both to verify the damaged nucleotide and to establish which strand has been damaged (14–16). Another important function of UvrB is recruitment of the UvrC protein that contains two functional endonuclease domains. The N-terminal part cuts the damaged strand four or five nucleotides 3′ to the lesion, whereas the

[1]Abbreviations: NER, nucleotide excision repair; AAF, *N*-acetyl-2-aminofluorene; T[6,4]T, pyrimidine–pyrimidone 6-4 photoproduct; G[8,5-Me]T, guanine–thymine intrastrand cross-link with a covalent bond between the C8 of guanine and the 5-methyl carbon of the 3′-thymine (please note that T[6,4]T and G[8,5-Me]T have also been used to represent the corresponding 2′-deoxydinucleoside monophosphate or DNA fragment); UvrABC, UvrA, UvrB, and UvrC proteins; EMSA, electrophoresis gel mobility shift assays; EDTA, ethylenediaminetetraacetic acid; TBA, Tris–boric acid–ethylenediaminetetraacetic acid; IPTG, isopropyl thiogalactoside; DTT, dithiothreitol; PAGE, polyacrylamide gel electrophoresis.

C-terminal part induces the second incision approximately eight nucleotides 5′ to the damaged nucleotide (12, 13). Previous studies on vicinal cross-links indicate that different intrastrand cross-links are incised at vastly different rates by UvrABC. For example, of the various UV thymine–thymine photoproducts, UvrABC removes the cis-syn, trans-syn, pyrimidine–pyrimidone 6-4 photoproduct (T[6,4]T), and Dewar photoproducts at relative rates of 1:6:9:9, respectively (17). Using a series of substrates, the investigators also established that the effect of neighboring sequences on repair of cis-syn thymine–thymine photodimer is relatively small (17). While this study showed that there is no correlation between the rates of repair and the degree of perturbation by these photoproducts, a more recent study using 2-, 3-, and 4-carbon tethers between the N^2 positions of two guanines showed that UvrABC recognition and incision are directly related to the degree of bending induced by the linker (18). The apparent disagreement between these studies reflects the difficulty in postulating a unified mechanism of UvrABC in repairing both monoadducts and cross-links, and more investigations on a variety of substrates would be needed to decipher the mechanistic details of this excision nuclease.

Whether the radiation-induced tandem lesions, such as G[8,5-Me]T, are repaired by NER is evidently an important question to be addressed. In addition, the availability of this new series of vicinal cross-links now provides another group of substrates to investigate the mechanism of UvrABC repair. Herein, we report that the G[8,5-Me]T cross-link is subject to repair, albeit not very efficiently, by UvrABC.

Materials and Methods

Chemicals and Enzymes

Tris base, boric acid, and ethylenediaminetetraacetic acid (EDTA) were purchased from Sigma (St. Louis, MO). Acrylamide, ammonium persulfate, *N*,*N*′-methylene bis-acrylamide, and urea were obtained from International Diagnostic (St. Joseph, MI). [γ-^{32}P]ATP was purchased from Amersham Biosciences (Piscataway, NJ). All other chemicals were obtained from Fisher Scientific (Fairlawn, NJ). Nuclease P1 and phosphodiesterase II were obtained from US Biological Inc. (Swampscott, MA), and phosphodiesterase I was from USB Corp. (Cleveland, OH). Bacterial alkaline phosphatase was purchased from Invitrogen Corp. (Carlsbad, CA). Restriction enzymes were obtained from New England Biolabs (Beverly, MA).

DNA Oligodeoxynucleotides

The T[6,4]T oligonucleotide was synthesized by Protein Chemistry Core Laboratory, University of Texas Medical Branch (Galveston, TX). The *N*-acetyl-2-aminofluorene (AAF)-11-mer was synthesized, purified, and characterized as described (19, 20). Each oligonucleotide was purified by urea polyacrylamide gel electrophoresis (PAGE) under denaturing conditions.

Protein Purification and Substrate Construction

The UvrA, UvrB, and UvrC proteins (UvrABCs) were overexpressed and purified from *E. coli* as described previously (19). Figure 1A shows the purified UvrABCs on an 8% SDS–

PAGE gel stained with Coomassie blue. The estimated purity of three proteins was more than 95%. The protein concentration was determined by Bio-Rad protein assay using BSA as a standard following the manufacturer's procedures. To investigate the interaction of *E. coli* UvrABC proteins with G[8,5-Me]T intrastrand cross-link adduct in comparison with T[6,4]T intrastrand cross-link adduct and AAF, DNA substrates of 49–51 bp were constructed containing a single adduct of G[8,5-Me]T, T[6,4]T, or AAF in the middle of the sequence (Figure 1B,C) (19). The control and lesion-containing oligonucleotides (i.e., an unmodified 12-mer, G[8,5-Me]T-12-mer, AAF-11-mer, or T[6,4]T-10-mer) were ligated to a 20-mer and 19-mer on the 5′- and 3′-ends, respectively, to generate the substrates (Figure 1C). For substrate construction with T[6,4]T and AAF, the 20-mer was 5′-terminally labeled with ^{32}P, while for G[8,5-Me]T, the G[8,5-Me]T-12-mer was 5′-terminally radiolabeled (thus, the 51 bp substrate was internally labeled). Relatively mild conditions (e.g., DNA was denatured at 80 °C for annealing rather than at >90 °C) were used to prevent G[8,5-Me]T and T[6,4]T cross-link and AAF adducts from any potential chemical alteration during preparation. The ligation products were purified by urea-PAGE under denaturing conditions. As shown in Supporting Information Figure S1A for the products of a typical ligation of the oligomers with the 5′-terminally labeled 20-mer, good yields of ligation have been obtained for all four substrates (as marked as 51-, 50-, and 49-mer). After the purification, the ligated products 51-mer, 50-mer, and 49-mer were annealed with their corresponding complementary strands (bottom 51-mer, 50-mer, and 49-mer) and purified again on an 8% polyacrylamide native gel. To confirm that all of the substrates were fully double strand and homogeneous, the substrates were subjected to digestion with restriction enzyme *Hae*III (Supporting Information Figure S1B) or *Res*I (data not shown). *Hae*III, which specifically recognizes DNA sequence 5′-GGCC-3′ (Figure 1C), efficiently cleaved these substrates to 41-mer, 40-mer, or 39-mer and 10-mer. All substrates were digested to >95% as indicated by loss of the top band and appearance of shorter oligonucleotides in the digestion products (Supporting Information Figure S1B). The restricted 10-mer was invisible on the gel since all samples shown in Supporting Information Figure S1 were 5′-terminally labeled.

Construction of DNA bubble substrates was carried out similarly as described above except that the damaged top strands were annealed with the bottom strands with the bases mismatched from the 2nd nucleotide 5′ through the 3rd (for AAF) or 2nd nucleotide (for G[8,5-Me]T and T[6,4]T) 3′ to the adduct (19). All bubble substrates were constructed with ^{32}P-labeling at the 5′-end of the starting 20-mer.

Electrophoretic Mobility Shift Assays (EMSA)

Binding of the UvrA protein to the DNA substrates was determined by gel mobility shift assays. Typically, the substrate (1 nM) was incubated with UvrA at varying concentrations as indicated at 37 °C for 15 min in 20 μL of UvrABC buffer [50 mM Tris-HCl, pH 7.5, 50 mM KCl, 10 mM $MgCl_2$, and 5 mM dithiothreitol (DTT)]. After incubation, 2 μL of 80% (v/v) glycerol was added, and the mixture was immediately loaded onto a 3.5% native polyacrylamide gel in 1 × TBE running buffer and electrophoresed at room temperature. For estimation of the dissociation constant for the UvrA interaction with a DNA adduct, radioactivity of the DNA bands on gel was quantified with a Fuji FLA-5000 phosphoimage scanner. The binding isotherm was then generated, and the K_d (dissociation constant) was

estimated from the UvrA titration concentration at which half of the DNA substrate molecules had been bound. The binding of UvrA and UvrB proteins to DNA substrates was carried out as described previously (21). Briefly, the mixture of proteins was incubated with DNA (1 nM) at 37 °C for 30 min in UvrABC binding buffer containing 1 mM ATP. The binding products were then separated on a 6% polyacrylamide native gel at room temperature with ATP (1 mM) and $MgCl_2$ (10 mM) present in both the gel and the 1 × TBE running buffer.

Incision Assays

The 5′-terminally labeled DNA substrates (2 nM) were incised by UvrABC (UvrA, 15 nM; UvrB, 250 nM; and UvrC, 100 nM) in the UvrABC buffer with 1 mM ATP at 37 °C for a given period. The UvrABC subunits were diluted and premixed into storage buffer before mixing with DNA substrates. The mixtures of UvrABC were loaded into the cap well of the reaction tube. Reactions were started by spinning the proteins down to the reaction buffer containing DNA substrate at the bottom of the tube. The reaction aliquots collected at each time point were terminated by adding EDTA (20 mM) and heating with formamide to 90 °C for 3 min. The samples were then analyzed by electrophoresis on a 12% polyacrylamide sequencing gel under denaturing conditions with 1 × TBE buffer.

Quantification of Incision Products

In this study, all quantitative data of radioactivity were generated using Image Reader FLA-5000 V2.0 and Image Gauge V3.46 and using the volume integration method. The amount of DNA incised (DI, in pmol) by UvrABC was calculated based on the total molar amount of DNA used in each reaction (M) and the percentage of radioactivity in the incision products (IP) as compared to the total radioactivity. At least three independent experiments were performed for determination of the rates of incision. The initial rate was determined by a linear least-squares fit of the data collected over the incision period.

Results and Discussion

Synthesis of G[8,5-Me]T Dodecamer

The monomer, 5′-dimethoxytrityl-5-(phenylthiomethyl)-2′-deoxyuridine phosphoramidite, was synthesized as described (6, 22). It was incorporated into the 12-mer, 5′-GTG CGU^{CH_2SPh} GTT TGT-3′, by “pac phosphoramidite” chemistry and deprotected under mild conditions (23). UV-C irradiation of this 12-mer (Figure 2A) gave a mixture of peaks by reverse phase HPLC (Figure 2B). ESI-MS analysis indicated that peaks a and b with abundant M − H mass peaks of 3693.56 and 3693.62, respectively, contained the G[8,5-Me]T or T[5-Me,8]G cross-link (calculated [M − H] is 3693.61), whereas the major peak c was found to contain the unmodified 12-mer, 5′-GTG CGT GTT TGT-3′. The remaining U^{CH_2SPh}-containing dodecamer eluted as peak d. Enzymatic digestion followed by reverse phase HPLC analysis showed that peak b contained the G[8,5-Me]T cross-link (Figure 3A). The presence of G[8,5-Me]T dinucleoside monophosphate was confirmed by mass spectral analysis, which showed a peak of 570.14 in positive ion mode and 568.09 in negative ion mode (calculated [M + H] and [M − H] are 570.14 and 568.12, respectively). The MS-MS analysis of the 570.14 and 568.09 peaks showed the formation of a fragment of *m*/*z* 276 and

274, respectively, corresponding to the guanine–thymine cross-linked base moiety and a fragment of *m*/*z* 472 and 470, respectively, corresponding to the loss of 2-deoxyribose (see Supporting Information Figures S3 and S4). This peak also coeluted with an authentic G[8,5-Me]T standard (Figure 3B). We found an additional peak X in the enzymatic digestion mixture, which eluted immediately before dC by reverse phase HPLC (Figure 3A). This peak exhibited an identical absorption spectrum as G[8,5-Me]T. A larger fraction of this peak was detected when the G[8,5-Me]T-containing dodecamer was subjected to digestion with only phosphodiesterase I and bacterial alkaline phosphatase. However, phosphodiesterase I (or II) and alkaline phosphatase had no effect on the G[8,5-Me]T dimer. ESI-MS analysis of X showed a peak of [M − H] 648.3 corresponding to a G[8,5-Me]T dimer with an additional phosphate. MS-MS analysis of this peak showed the expected peaks of 568, 470, and 274 corresponding to G[8,5-Me]T and its fragments. Taken together, we conclude that X contained G[8,5-Me]T 5′-phosphate, which resulted from incomplete hydrolysis of the 5′-phosphate by bacterial alkaline phosphatase.

Binding of UvrA to G[8,5-Me]T in Comparison to T[6,4]T Intrastrand Cross-Link and dG-AAF–DNA Adduct

To understand the biochemical basis of recognition and incision of G[8,5-Me]T cross-link by UvrABC nucleases, we performed gel mobility shift assays to examine binding of these DNA substrates with varying concentrations of UvrA. As a positive control, we used the T[6,4]T photoproduct (Figure 1B), which is a vicinal cross-link and is known to be a good substrate for UvrABC. It is repaired nine times more efficiently by UvrABC than cis-syn thymine–thymine photodimer (17). We also used a highly distorting AAF monoadduct of dG (Figure 1B) as another positive control. It is noteworthy that the local DNA sequences for the T[6,4]T and dG-AAF used here were different (Figure 1C), but we believe that the context difference is unlikely to have a major effect. This is based on a sequence context study of thymine–thymine cis-syn photodimer, which showed that the sequence effect on the Uvr repair is relatively small (17). With dG–AAF and dG–AF adducts, we also found that both UvrA binding and UvrABC incisions could change in a different sequence context, but the magnitude is within 2-fold (24). It is important to point out that the AAF adduct at the *Nar*I site (5′-$G_1G_2CG_3$-CC-3′) shows a more pronounced effect on the efficiency of incision: The adducts at G_1 and G_3 are incised at a much greater efficiency than the adduct at G_2 (25). However, a strong sequence-dependent polymorphism of the adduct and existence of multiple conformations that interconvert rapidly in the *Nar*I sequence have been suggested to contribute toward these differences in the NER.

As shown in Figure 4, incubation of these substrates with UvrA resulted in formation of the $UvrA_2$–DNA complex as a slowly mobilizing band. The faster running band represented the substrate free of UvrA protein. Titration of the binding with varying UvrA concentrations generated binding isotherms, which were then used for determination of the dissociation constants (19). As listed in Table 1, the order of binding affinity was G[8,5-Me]T ≈ T[6,4]T ≫ AAF. As expected, the affinity of UvrA for nondamaged 51bp was much lower than damaged DNA (Figure 4C, lanes 1–4). Because the $UvrA_2$ protein is responsible for the recognition of local DNA helix alterations such as bending, kinking, and unwinding induced by DNA adduct (12, 13, 26), the higher affinities of UvrA for the G[8,5-Me]T and T[6,4]T

intrastrand cross-linked substrates suggest that relative to the AAF adduct, a more pronounced helical distortions of DNA duplex might have been induced by the cross-links. It is important to point out that in comparison to several other bulky C8–dG monoadducts, AAF adduct is recognized more efficiently by UvrA (19), which implies that UvrA recognition of these two vicinal cross-links is remarkably efficient.

UvrABC Incisions of G[8,5-Me]T, T[6, 4]T Intrastrand Cross-link and AAF DNA Substrates

As shown in Figure 5A,B, the three substrates containing G[8,5-Me]T, T[6,4]T intrastrand cross-links and AAF–C8 guanine adduct (structures shown in Figure 1B) were incised by UvrABC nuclease in a kinetic assay. These substrates were either labeled at the 5′-end of the damaged strand (for T[6,4]T and AAF) or internally labeled (for G[8,5-Me]T) (see Materials and Methods), and thus, different lengths of radiolabeled incision products were observed. A major incision product of labeled 13-mer was visualized on gel for G[8,5-Me]T-51bp substrate (Figure 5A), while 18-mer and 17-mer products were obtained with AAF-50bp and T[6,4]T-49bp substrates, respectively (Figure 5B). This result is consistent with the currently accepted mechanism of UvrABC, in which $UvrA_2B$ complex binds to the cross-linked or lesion-containing DNA. The $UvrA_2$ protein then dissociates, and UvrC is recruited. For the G[8,5-Me]T substrate, because the substrate was internally labeled, the observed incision product is the radiolabeled 13-mer containing the G[8,5-Me]T adduct. Thus, it appears that the first primary incision occurs between the 4th and the 5th bases 3′ to the lesion, which is followed by the second incision eight phosphates 5′ to the cross-link (generating a radiolabeled 13-mer).

The result also indicates that the repair proteins cleaved G[8,5-Me]T, T[6,4]T, and AAF adducts with significantly different efficiencies. Particularly notable was the difference in incision rates between the two cross-links. As shown in Table 1, the incision rates follow the order of T[6,4]T > AAF ≫ G[8,5-Me]T. Although G[8,5-Me]T and T[6,4]T intrastrand cross-linked substrates were recognized equally well by the UvrA protein (Figure 4 and Table 1), the UvrABC incision of G[8,5-Me]T cross-link was far less efficient than that of T[6,4]T. It has been postulated that DNA damages are recognized by UvrABC through at least two sequential and dynamic steps, in which the first step involves recognition of DNA helical distortion, whereas the second one involves recognition of the adduct structure and conformation in the single-stranded region of DNA (13, 26, 27). Therefore, our results could be attributed to poor recognition of the G[8,5-Me]T lesion at the second step in which UvrB plays a crucial role in recognition following the UvrA binding, with the resultant effect that the adduct was incised inefficiently. It also suggests that the second step of recognition may be more important than the first one for the UvrABC repair efficiency. Additional supporting evidence was obtained from the UvrABC incisions of DNA bubble substrates. Unlike the normal DNA substrates, the presence of bubble structure with mismatched bases flanking the lesion has been used to override the helical distortion induced by the DNA damage as well as the UvrA-induced first step of recognition (12, 13). As shown in Figure 6, the G[8,5-Me]T adduct was incised with a much lower efficiency as compared to the other two lesions. We wish to point out that the additional incision products of 10-mer and 11-mer observed in Figure 6 were due to the 2nd 5′-incision of UvrABC (12, 28, 29). This second

incision is coupled with and depended on the first 5′-incisions and therefore should be included for determination of incision efficiencies (13).

To further confirm the poor recognition by UvrB, formation of UvrB–DNA complex in the binding of UvrA and UvrB proteins to substrates was examined in a gel mobility shift assay in the presence of ATP (Figure 7). Consistent with the other experiments, the efficiency of the complex formation followed the order T[6,4]T > AAF ≫ G[8,5-Me]T. In fact, little UvrB–G[8,5-Me]T complex could be visualized on the gel even after prolonged exposure (Figure 7). The structural feature of the G[8,5-Me]T cross-link that results in poor UvrB–adduct interaction remains to be investigated in the future. However, it is reasonable to speculate that the chemical structure and conformation of the lesion-containing mono- (in AAF) or binucleotide (in the cross-links) play a role in the stability of the UvrB–DNA complex. As compared to T[6,4]T, which is very rigid and induces a series of changes in sugar pucker and torsion angles (30, 31), the G[8,5-Me]T cross-link incurs little structural changes in DNA. In addition, hydrophobicity is believed to be an important property recognized by UvrB (13, 21), and evidently, as compared to the AAF adduct, G[8,5-Me]T is much less hydrophobic. Thermal melting experiments with DNA containing a G[8,5]C cross-link, a lesion structurally similar to G[8,5-Me]T, showed that it induces only modest destabilization of the DNA duplex similar to 8-oxoguanine or thymine glycol (5). A preliminary modeling study of G[8,5-Me]T in duplex form showed that, unlike the T[6,4]T and the AAF adduct, all of the hydrogen bonds of the guanine and the thymine of G[8,5-Me]T can be maintained, even though a kink in the helix axis was unavoidable (Figure 8). Studies are ongoing to address some of the structural issues of this cross-link. However, the fact that G[8,5-Me]T cross-link was much more resistant to UvrABC incisions and thus to NER as compared to the two other lesions studied here implies that this type of DNA damage would probably persist longer in *E. coli* cells.

Supplementary Material

Refer to Web version on PubMed Central for supplementary material.

Acknowledgments

We thank Marina Dickens (NSF sponsored 2004 summer REU student at the University of Connecticut) (supported by Grant CHE 523532) for technical assistance. We are indebted to M. Abul Kalam (University of Connecticut) for conducting the preliminary modeling study. This study was supported by NCI Grant CA86927 (Y.Z.) and NIEHS Grant ES09127 (A.K.B.)

References

1. Friedberg, EC.; Walker, GC.; Siede, W. DNA Repair and Mutagenesis. ASM Press; Washington, DC: 1995.
2. Huttermann, J.; Kuhnlein, W.; Téoule, R. Effects of Ionizing Radiation on DNA Physical, Chemical, and Biological Aspects. Springer-Verlag; Berlin: 1978.
3. Goodhead DT. Initial events in the cellular effects of ionizing radiation: Clustered damage in DNA. Int J Radiat Biol. 1994; 65:7–17. [PubMed: 7905912]
4. Box HC, Patrzyc HB, Dawidzik JB, Wallace JC, Freund HG, Iijima H, Budzinski EE. Double base lesions in DNA X-irradiated in the presence or absence of oxygen. Radiat Res. 2000; 153:442–446. [PubMed: 10761005]

5. Gu C, Wang Y. LC-MS/MS Identification and yeast polymerase η bypass of a novel γ-irradiation-induced intrastrand cross-link lesion G[8-5]C. Biochemistry. 2004; 43:6745–6750. [PubMed: 15157108]
6. Zhang Q, Wang Y. Independent generation of 5-(2′-deoxycytidinyl)methyl radical and the formation of a novel cross-link lesion between 5-methylcytosine and guanine. J Am Chem Soc. 2003; 125:12795–12802. [PubMed: 14558827]
7. Zhang Q, Wang Y. Independent generation of the 5-hydroxy-5,6-dihydrothymidin-6-yl radical and its reactivity in dinucleoside monophosphates. J Am Chem Soc. 2004; 126:13287–13297. [PubMed: 15479083]
8. Zhang Q, Wang Y. Generation of 5-(2′-deoxycytidyl)-methyl radical and the formation of intrastrand cross-link lesions in oligodeoxyribonucleotides. Nucleic Acids Res. 2005; 33:1593–1603. [PubMed: 15767284]
9. Box HC, Dawidzik JB, Budzinski EE. Free radical-induced double lesions in DNA. Free Radical Biol Med. 2001; 31:856–868. [PubMed: 11585704]
10. Hazra T, Izumi T, Kow YW, Mitra S. The discovery of a new family of mammalian enzymes for repair of oxidatively damaged DNA, and its physiological implications. Carcinogenesis. 2003; 24:155–157. [PubMed: 12584162]
11. Brooks PJ, Wise DS, Berry DA, Kosmoski JV, Smerdon MJ, Somers RL, Mackie H, Spoonde AY, Ackerman EJ, Coleman K, Tarone RE, Robbins JH. The oxidative DNA lesion 8,5′-(S)-cyclo-2′-deoxyadenosine is repaired by the nucleotide excision repair pathway and blocks gene expression in mammalian cells. J Biol Chem. 2000; 275:22355–22362. [PubMed: 10801836]
12. Zou Y, Van Houten B. Strand opening by the UvrA2B complex allows dynamic recognition of DNA damage. EMBO J. 1999; 18:4889–4901. [PubMed: 10469667]
13. Zou Y, Luo C, Geacintov NE. Hierarchy of DNA damage recognition in *Escherichia* coli nucleotide excision repair. Biochemistry. 2001; 40:2923–2931. [PubMed: 11258904]
14. Theis K, Chen PJ, Skorvaga M, Vna Houten B, Kisker C. Crystal structure of UvrB, a DNA helicase adapted for nucleotide excision repair. EMBO J. 1999; 18:6899–6907. [PubMed: 10601012]
15. Skorvaga M, Theis K, Mandavilli BS, Kisker C, Van Houten B. The beta-hairpin motif of UvrB is essential for DNA binding, damage processing, and UvrC-mediated incisions. J Biol Chem. 2002; 277:1553–1559. [PubMed: 11687584]
16. Van Houten B, Eisen JA, Hanawalt PC. A cut above: Discovery of an alternative excision repair *pathway in bacteria*. Proc Natl Acad Sci USA. 2002; 99:2581–2583. [PubMed: 11880612]
17. Svoboda DL, Smith CA, Taylor JSA, Sancar A. Effect of sequence, adduct type, and opposing lesions on the binding and repair of ultraviolet photodamage by DNA photolyase and (A)BC excinuclease. J Biol Chem. 1993; 268:10694–10700. [PubMed: 8486719]
18. Kowalczyk A, Carmical JR, Zou Y, Van Houten B, Lloyd RS, Harris CM, Harris TM. Intrastrand DNA cross-links as tools for studying DNA replication and repair: Two-, three-, and four-carbon tethers between the N^2 positions of adjacent guanines. Biochemistry. 2002; 41:3109–3118. [PubMed: 11863450]
19. Luo C, Krishnasamy R, Basu AK, Zou Y. Recognition and incision of site-specifically modified C8 guanine adducts formed by 2-aminofluorene, *N*-acetyl-2-aminofluorene and 1-nitropyrene by UvrABC nuclease. Nucleic Acids Res. 2000; 28:3719–3724. [PubMed: 11000263]
20. Liu Y, Yang Z, Utzat CD, Liu Y, Geacintov NE, Basu AK, Zou Y. Interactions of human replication protein A with single-stranded DNA adducts. Biochem J. 2005; 385:519–526. [PubMed: 15362978]
21. Zou Y, Ma H, Minko IG, Shell SM, Yang Z, Qu Y, Xu Y, Geacintov NE, Lloyd RS. DNA damage recognition of mutated forms of UvrB proteins in nucleotide excision repair. Biochemistry. 2004; 43:4196–4205. [PubMed: 15065863]
22. Romieu A, Bellon S, Gasparutto D, Cadet J. Synthesis and UV photolysis of oligodeoxynucleotides that contain 5-(phenylthiomethyl)-2′-deoxyuridine: A specific photolabile precursor of 5-(2′-deoxyuridilyl)methyl radical. Org Lett. 2000; 2:1085–1088. [PubMed: 10804560]

23. Bellon S, Ravanat JL, Gasparutto D, Cadet J. Cross-linked thymine-purine base tandem lesions: Synthesis, characterization, and measurement in γ-irradiated isolated DNA. Chem Res Toxicol. 2002; 15:598–606. [PubMed: 11952347]
24. Zou Y, Shell SM, Utzat CD, Luo C, Yang Z, Geacintov NE, Basu AK. Effects of DNA adduct structure and sequence context on strand opening of repair intermediates and incision by UvrABC nuclease. Biochemistry. 2003; 42:12654–12661. [PubMed: 14580212]
25. Delagoutte E, Bertrand-Burggraf E, Dunand J, Fuchs RPP. Sequence-dependent modulation of nucleotide excision repair: The efficiency of the incision reaction is inversely correlated with the stability of the pre-incision UvrB-DNA complex. J Mol Biol. 1997; 266:703–710. [PubMed: 9102463]
26. Van Houten B. Nucleotide excision repair in *Escherichia coli*. Microbiol Rev. 1990; 54:18–51. [PubMed: 2181258]
27. Van Houten B, Snowden A. Mechanism of action of the *Escherichia coli* UvrABC nuclease: Clues to the damage recognition problem. Bioessays. 1993; 15:51–59. [PubMed: 8466476]
28. Gordienko I, Rupp WD. A specific 3′ exonuclease activity of UvrABC. EMBO J. 1998; 17:626–633. [PubMed: 9430653]
29. Moolenaar GF, Bazuine M, van Knippenberg IC, Visse R, Goosen N. Characterization of the *Escherichia coli* damage-independent UvrBC endonuclease activity. J Biol Chem. 1998; 273:34896–34903. [PubMed: 9857018]
30. Taylor JS, Garrett DS, Wang MJ. Models for the solution state structure of the (6-4) photoproduct of thymidylyl-(3′→5′)-thymidine derived via a distance- and angle-constrained conformation search procedure. Biopolymers. 1988; 27:1571–1593. [PubMed: 3233321]
31. Dupradeau FY, Sonnet P, Guillaume D, Senn HM, Clivio P. Ab initio study of the (5*R*)- and (5*S*)-TT pyrimidine h^5(6-4) pyrimidone photoproducts. Implications on the design of new biologically relevant analogues. J Org Chem. 2002; 67:9140–9145. [PubMed: 12492313]

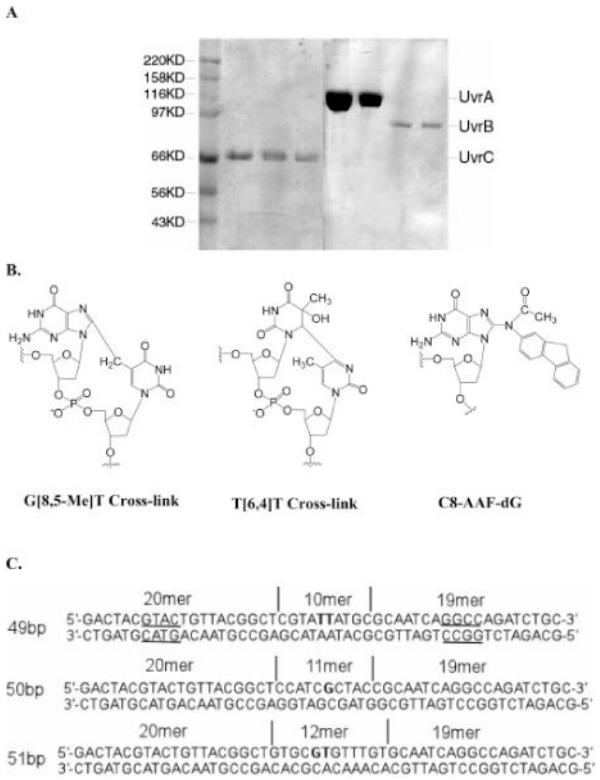

Figure 1.

Protein purification and structures of DNA substrates used in this study. (A) Purified UvrABCs as analyzed on a 8% SDS–PAGE. (B) Chemical structures of G[8,5-Me]T and T[6,4]T intrastrand cross-link and AAF adduct. (C) Sequences of the constructed DNA substrates for use. The bolded nucleotides represent the damaged ones. The recognition sequences of restriction endonuclease have been underscored.

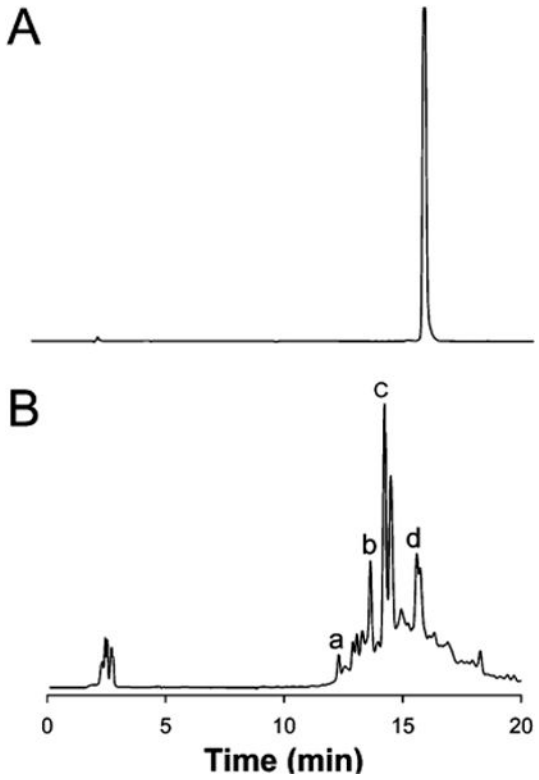

Figure 2.

Reverse phase HPLC profiles of $_{U}^{CH_2SPh}$ containing dodecamer (A) before and (B) after UV-C radiation for 6 min at 25 °C. HPLC conditions: For panels A and B, Phenomenex Ultracarb C18 (7 μm) (250 mm × 4.6 mm) column, 0.1 M ammonium acetate buffer (pH 6.8) with a gradient of 1–32% acetonitrile in 30 min at a flow rate 1 mL/min.

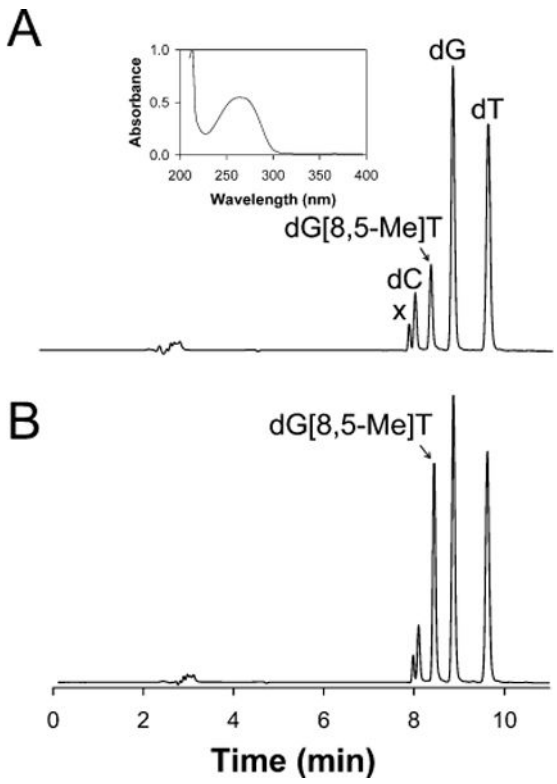

Figure 3.

(A) Reverse phase HPLC analysis of cross-linked 12-mer (peak b in Figure 2) after digestion with nuclease P1, bacterial alkaline phosphatase, and phosphodiesterases I and II. The inset in panel A shows the absorption spectrum of G[8,5-Me]T. (B) The same coinjected with a G[8,5-Me]T dinucleoside monophosphate standard. The oligonucleotide (20 μg) was dissolved in 100 μL of aqueous solution containing 50 mM sodium acetate, 30 mM sodium chloride, and 1.0 mM zinc sulfate (pH 4.5) and treated with 2 U of nuclease P1 and 0.03 U of phosphodiesterase II. The reaction mixture was incubated at 37 °C for 12 h and at room temperature for another 12 h. It was then dried and redissolved in 60 μL of Tris-HCl (500 mM, pH 8.5). The solution was then treated with 40 U of bacterial alkaline phosphatase and 0.1 U of phosphodiesterase I. The digestion mixture was again incubated at 37 °C for 12 h and at room temperature for another 12 h. It was concentrated in vacuo, redissolved in 100 μL of water, and extracted with chloroform (3×). The aqueous layer was dried and redissolved in water, and an aliquot was injected into HPLC for analysis. HPLC conditions: Ultracarb C18 (5 μm) (250 mm × 4.6 mm) column, 0.1 M ammonium acetate buffer (pH 5.5) with a gradient of 1–32% acetonitrile in 15 min at a flow rate of 1 mL/min.

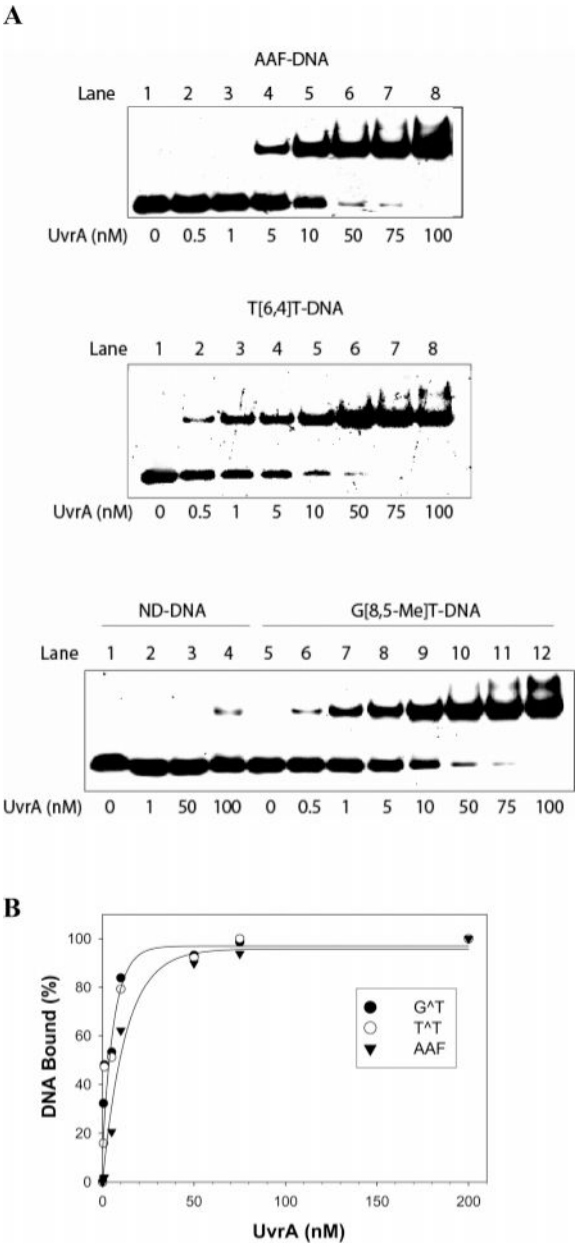

Figure 4.

Binding of UvrA to G[8,5-Me]T-51bp, AAF-50bp, and T[6,4]T-49bp substrates. (A) UvrA at the concentration specified was incubated at 37 °C for 10 min with 1 nM G[8,5-Me]T cross-link-51bp, AAF-50bp, or T[6,4]T cross-link-49bp substrate in UvrABC binding buffer and then analyzed on a 3.5% polyacrylamide native gel by gel mobility shift assays. (B) The binding isotherms generated from the titration data in panel A.

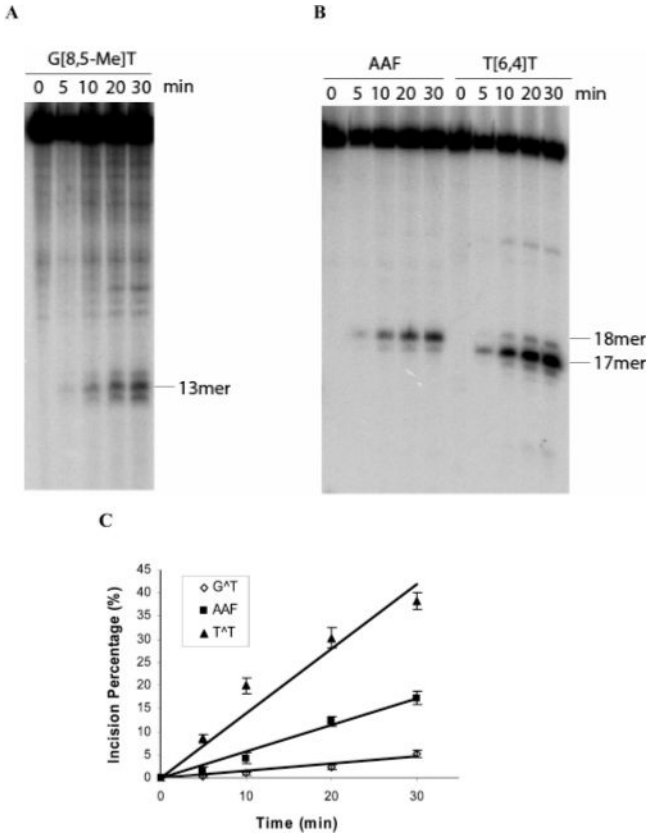

Figure 5.

Incision of AAF-50bp, T[6,4]T-49bp, and G[8,5-Me]T-51bp substrates by UvrABC nuclease. Panel A shows the incision of the G[8,5-Me]T substrate that was internally labeled with ^{32}P at the 5th nucleotide 5′ to the cross-linked site. Panel B shows the incisions of the T[6,4]T cross-link and AAF adduct-containing substrates that were 5′-terminally labeled with ^{32}P. In both panels A and B, the DNA substrates were incubated with UvrABC proteins in the UvrABC buffer in the presence of 1 mM ATP at 37 °C for the periods as indicated. The reaction products were analyzed on a 12% urea PAGE under denaturing conditions. (C) Kinetics of UvrABC incisions of DNA substrates.

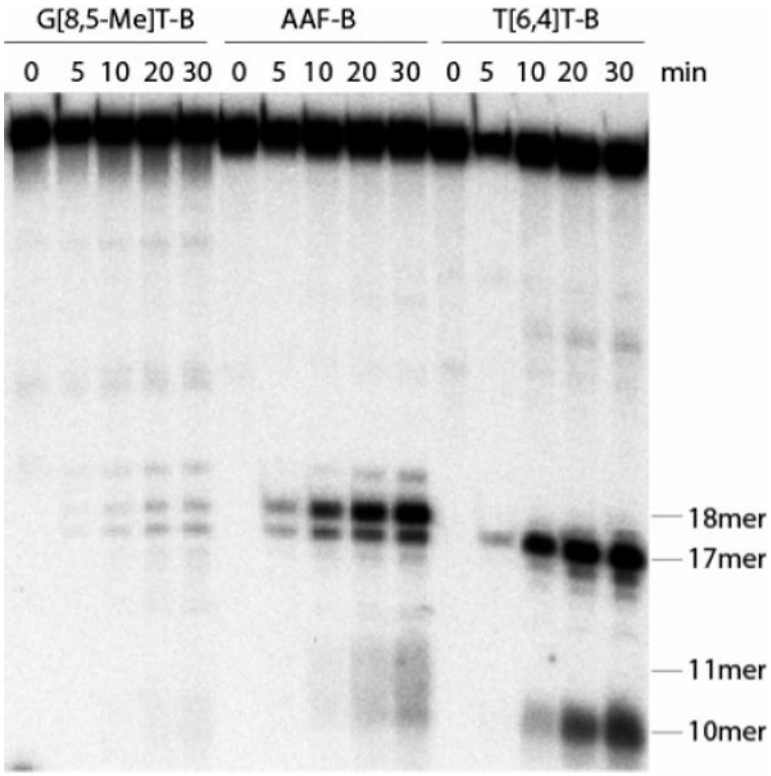

Figure 6.

Incision of AAF-, T[6,4]T-, and G[8,5-Me]T-DNA bubble substrates by UvrABC nuclease. The DNA substrates were incubated with UvrABC proteins in the UvrABC buffer in the presence of 1 mM ATP at 37 °C for the periods as indicated. The reaction products were analyzed on a 12% urea PAGE under denaturing conditions. All substrates were 5′-terminally labeled with ^{32}P.

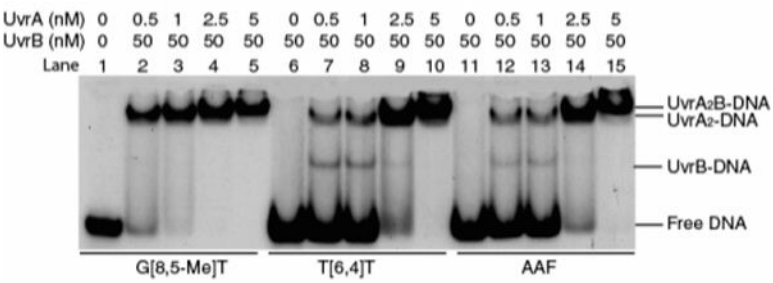

Figure 7.

Binding of UvrA and UvrB to G[8,5-Me]T-51bp, AAF-50bp, and T[6,4]T-49bp substrates. UvrA and UvrB at concentrations specified were incubated at 37 °C for 30 min with 1 nM DNA G[8,5-Me]T cross-link-51bp, AAF-50bp, or T[6,4]T cross-link-49bp substrate in UvrABC binding buffer containing 1 mM ATP. The products were analyzed on a 6% polyacrylamide native gel in the presence of 1 mM ATP.

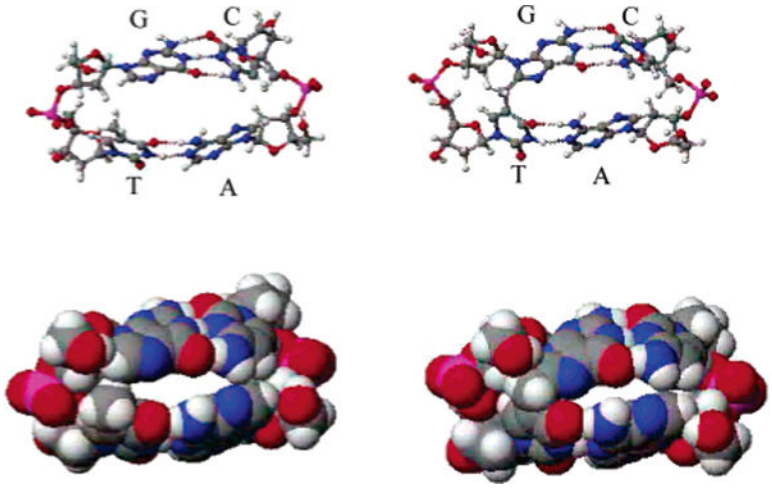

Figure 8.

Left and right panels show the unmodified 5′-GT-3′ and 5′-G[8,5-Me]T-3′ models, respectively, in duplex form. The duplexes were built using the average values of torsion angles and atomic distances of the B-DNA. Because the counterions near the phosphate group of sugar–phosphate backbone are believed to have little effect on the structure of DNA, no counterions have been used in constructing the model complexes. PM3 method was used for the energy optimizations. The solvent effect was not considered in the calculations.

Table 1

Equilibrium Dissociation Constants for UvrA Binding to Different Damaged Substrates and Initial Rates of UvrABC Incisions of DNA Substrates at 37 °C[a]

substrate	K_d (nM)	initial incision rate (fmol/min)
G[8,5-Me]T-51bp	3.1 ± 1.3	0.17 ± 0.02
T[6,4]T-49bp	2.8 ± 0.9	1.34 ± 0.16
AAF-50bp	8.2 ± 1.9	0.53 ± 0.03

[a]Data represent the means ± SD of at least three independent experiments. The dissociation constants were determined for UvrA dimer unless otherwise indicated.